Constraints on possible phase transitions above the nuclear saturation density

I.N. Mishustin[1,2,3], **L.M. Satarov**[1,2], **H. Stöcker**[1], **and W. Greiner**[1]

[1] *Institut für Theoretische Physik, J.W. Goethe Universität, D–60054 Frankfurt am Main, Germany*
[2] *The Kurchatov Institute, Russian Research Center, 123182 Moscow, Russia*
[3] *The Niels Bohr Institute, DK–2100 Copenhagen Ø, Denmark*

Abstract

We compare different models for hadronic and quark phases of cold baryon–rich matter in an attempt to find a deconfinement phase transition between them. For the hadronic phase we consider Walecka–type mean–field models which describe well the nuclear saturation properties. We also use the variational chain model which takes into account correlation effects. For the quark phase we consider the MIT bag model, the Nambu–Jona-Lasinio and the massive quasiparticle models. By comparing pressure as a function of baryon chemical potential we find that crossings of hadronic and quark branches are possible only in some exceptional cases while for most realistic parameter sets these branches do not cross at all. Moreover, the chiral phase transition, often discussed within the framework of QCD motivated models, lies in the region where the quark phases are unstable with respect to the hadronic phase. We discuss possible physical consequences of these findings.

1 Introduction

It is commonly believed that quarks and gluons are relevant degrees of freedom in strongly interacting matter at very high temperatures and baryon densities. This state of matter is usually described by various QCD motivated models. On the other hand, at low temperatures and moderate densities, at least up to the nuclear saturation density $\rho_0 = 0.17$ fm^{-3}, strongly interacting matter exists in the hadronic phase. In particular, atomic nuclei are finite droplets of this phase with baryon density $\rho_B \simeq \rho_0$. They are self–bound and therefore can exist in vacuum, without external pressure. This fact itself provides an important constraint on the equation of state (EOS) of cold nuclear matter, namely, its pressure must vanish at $\rho_B = \rho_0$. There are many effective models which successfully describe nuclear matter in terms of interacting nucleons.

Unfortunately, at present there exists no rigorous approach which can describe the EOS of strongly interacting matter at finite baryon densities. As known, QCD lattice simulations have principal limitations at nonzero chemical potential. Therefore the only practical way to study the possibility of the deconfinement phase transition in this case is to compare various models of hadronic and quark phases. In the last two decades there were numerous attempts to construct a unified EOS which would interpolate between the two asymptotic regimes. In this paper we critically revise this problem in the light of new calculations for the hadronic and quark phases.

In our analysis we include four hadronic models. Two of them are Relativistic Mean–Field (RMF) models of the Walecka type [1, 2], namely, the NLZ [3] and the TM1 [4] models. Next is the so called Chiral Hadronic Model (CHM) which was recently developed in Refs. [5, 6]. Fourth model is the Variational Chain Model (VCM) [7] based on the Argonne NN potentials with addition of 3–body forces and relativistic corrections. Unlike the above three models, the VCM takes into account correlation effects neglected in the mean–field approximation. As argued in Ref. [7], the mean–field approximation is not well justified at baryon densities $\rho_B \lesssim \rho_0$.

For the quark matter we take three different models: the MIT Bag Model (BM) [8], the Massive Quasiparticle Model (MQM) [9, 10] and the Nambu–Jona-Lasinio model (NJL) [11, 12]. Presumably, the hadronic degrees of freedom are more relevant at baryon densities $\rho_B \lesssim \rho_0$ and quark degrees of freedom take over at much larger densities. But the transition between these two regimes is very poorly understood at present. By considering various hadronic and quark models we pursue several goals. First, we compare different models for a single phase to get an idea on the uncertainty in their predictions. Second, by applying the Gibbs criterion, we investigate the possibility of a deconfinement phase transition in cold baryon-rich matter. Finally, we examine reliability of different quark models (in particular, allowed values of model parameters) by extrapolating their predictions into the domain of nuclear matter, $\rho_B \sim \rho_0$.

The paper is organized as follows. In Sect. II we give short descriptions of several popular models of the hadronic phase. Their predictions regarding the equation of state of cold baryonic

matter are summarized and compared between each other.In Sect. III different models of the quark phase are introduced. Their pairwise comparison with hadronic models, aimed at finding a hadron–quark phase transition, is carried out in a systematic way. In Sect. IV we present our conclusions and outlook.

2 Models of hadronic phase

2.1 Relativistic mean–field models

At present the field–theoretical description of dense hadronic matter is one of the most popular approaches. Within this approach the matter is described in terms of baryons interacting with self–consistent meson fields. Most calculations are done within the mean–field approximation. There are many versions of the RMF model which differ by the choice of meson fields as well as by the baryon–meson coupling schemes. Here we consider two realizations of the RMF approach which give very good description of finite nuclei, namely, the NLZ [3] and the TM1 [4] models.

The general form of the effective RMF Lagrangian used in these models is [1]

$$\mathcal{L} = \overline{\psi}\left(i\partial\!\!\!/ - m_N^* - g_\omega \omega\gamma_0\right)\psi - U_s(\sigma) + U_v(\omega)\,. \tag{1}$$

Here ψ, σ and ω are, respectively, the nucleon, scalar and vector meson fields,

$$m_N^* = m_N - g_\sigma \sigma \tag{2}$$

is the effective nucleon mass, U_s and U_v are the scalar and vector potentials:

$$U_s(\sigma) = \frac{(m_\sigma \sigma)^2}{2} + \frac{g_2 \sigma^3}{2} + \frac{g_3 \sigma^4}{4}\,, \tag{3}$$

$$U_v(\omega) = \frac{(m_\omega \omega)^2}{2} + \frac{g_{3\omega} \omega^4}{4}\,. \tag{4}$$

In the above equations m_i denote vacuum masses of nucleons ($i = N$) and mesons ($i = \sigma, \omega$), g_j are coupling constants. The parameter sets for the NLZ and TM1 models are listed in Table 1. Note that contrary to the NLZ, within the TM1 model the vector field is a nonlinear

[1] Below we consider static and homogeneous isospin–symmetric matter. In this case the derivatives of mean meson fields over space and time as well as the contribution of ρ–mesons may be omitted.

function of the baryon density. This leads to a significant reduction of the repulsive interaction at high ρ_B.

Table 1: Parameters of RFM models

	$m_N\,(\mathrm{GeV})$	$m_\sigma\,(\mathrm{GeV})$	$m_\omega\,(\mathrm{GeV})$	g_σ	$g_2\ (\mathrm{fm}^{-1})$	g_3	g_ω	$g_{3\omega}$
NLZ [3]	938.9	488.67	780	10.0553	-13.5072	-40.2243	12.9086	0
TM1 [4]	938.0	511.198	783	10.0289	-7.2325	0.6183	12.6139	71.305

Within the mean–field approximation σ and ω fields are regarded as purely classical and replaced by c–numbers. Using the Lagrangian (1) one can easily calculate pressure P of cold nonstrange matter as a function of the baryon chemical potential μ_B (see for details Refs. [1, 2]). At given μ_B, applying thermodynamic relations one obtains the following equations for the baryon density and the energy density of matter

$$\rho_B = dP/d\mu_B\,, \tag{5}$$

$$\epsilon = \mu_B\rho_B - P\,. \tag{6}$$

The energy per baryon is equal to $E/B = \epsilon/\rho_B$.

2.2 The chiral hadron model

Although the Lagrangian (1) leads to very good description of nuclear phenomenology it has one principal defect. Namely, it does not respect chiral symmetry of strong interaction. It is commonly accepted that this symmetry is spontaneously broken in vacuum and can be restored at high density and temperature. In recent years there were several attempts to incorporate this symmetry into the RMF framework. It turned out that most easily this can be achieved [13, 14] by introducing an additional scalar (dilaton) field χ responsible for the trace anomaly of QCD. For our analysis we have chosen the Chiral Hadron Model (CHM) developed in Ref. [5, 6]. Below we use the version of the CHM, given by the parameter set C1 in Ref. [6]. As compared to the NLZ and TM1 models, the CHM includes also a strange scalar field ζ. The following parametrization of m_N^* is used instead of (2):

$$m_N^* = g_\sigma\sigma + g_\zeta\,. \tag{7}$$

The scalar potential U_s is parametrized as a fourth-order polynomial in σ, ζ and χ. Its parameters are tuned to reproduce the pattern of spontaneous symmetry breaking at low densities. In addition there appear logarithmic terms, $\propto \chi^4 \log \chi^4$ and $\propto \chi^4 \log (\sigma^2 \zeta)$, motivated by the trace anomaly. As shown in Ref. [6] the CHM gives satisfactory description of nuclear matter and finite nuclei.

2.3 The variational chain model

The VCM [7] is a microscopic approach where the interaction between nucleons is describes in terms of two and three body forces. The Hamiltonian is written in the form

$$\mathcal{H} = -\sum_i \frac{1}{4}\left(\frac{1}{m_p}+\frac{1}{m_n}\right)\Delta_i + \sum_{i<j}(v_{ij}+\delta v_{ij}) + \sum_{i<j<k} v_{ijk}\,. \tag{8}$$

Here the first term gives non–relativistic kinetic energy of nucleons. The NN interaction terms v_{ij} are chosen in the form of the Argonne potential with parameters fitted to reproduce the NN scattering phases up to the c.m. energy 300 MeV. The terms δv_{ij} denote relativistic (Lorentz–boost) corrections up to the second order in the NN pair momentum. The 3N interaction terms v_{ijk} are taken in the Urbana UIX form with parameters which correctly reproduce binding energies of lightest ($A \leq 4$) nuclei. The calculations are carried out by applying the variational Monte Carlo method and the chain summation technique [7]. Besides properties of finite nuclei, pressure and energy density of nuclear matter are calculated at various nucleon densities and neutron to proton ratios.

2.4 Comparison of model predictions

In Figs. 1–5 we compare pressure and binding energy of cold isospin–symmetric baryonic matter calculated within the above four models. Figure 1 shows predictions for energy per baryon as a function of ρ_B. All models give nearly the same results at densities $\rho_B \lesssim \rho_0$. At higher densities the CHM, VCM, and the TM1 model are not far from each other, unlike the NLZ model which seems to overestimate significantly the energy per baryon at $\rho_B \gtrsim 3\rho_0$ [2].

[2] One should regard the results of effective hadronic models at $\rho_B >> \rho_0$ with caution due to the lack of available information concerning EOS at such densities.

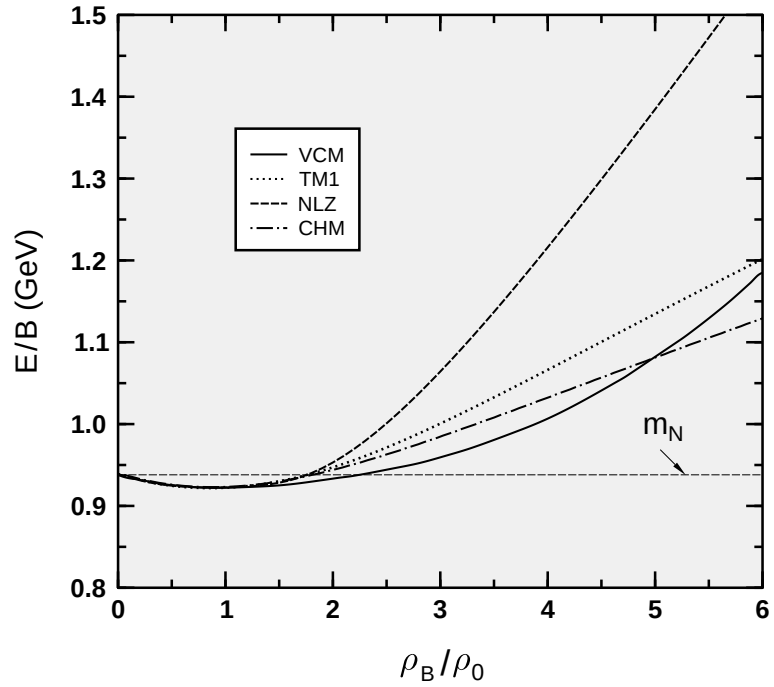

Figure 1: Energy per baryon of cold nuclear matter calculated within different hadronic models as function of baryon density. Here and below the curves are specified in the key box.

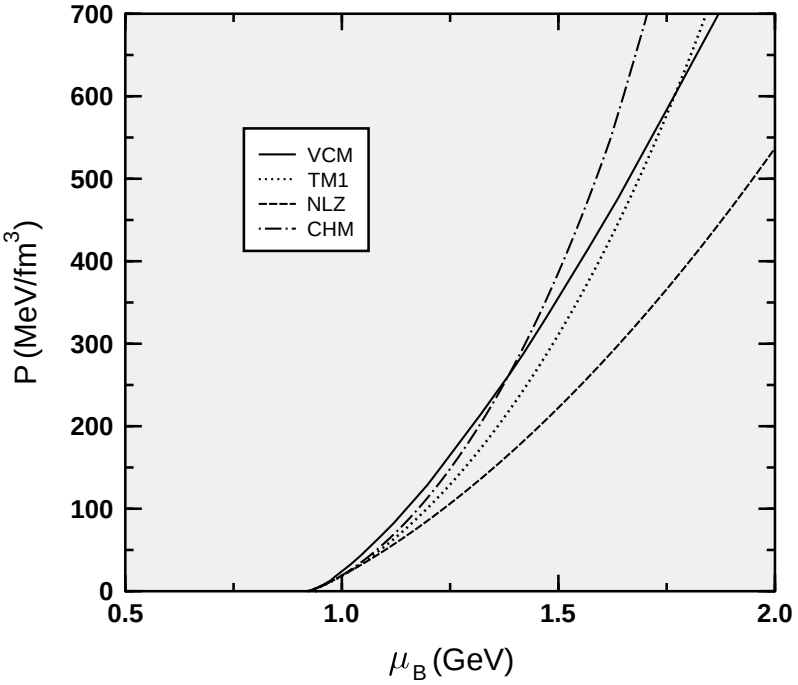

Figure 2: Pressure of cold nuclear matter vs baryon chemical potential calculated within different hadronic models.

Figure 2 shows pressure as a function of baryon chemical potential. The discrepancy between different hadronic models becomes especially evident at $\mu_B - m_N \gtrsim 200$ MeV. One can see that the results of the NLZ model strongly deviate from the predictions of other models. Apparently, this is due to overestimation of vector repulsion within the NLZ model. On the other hand, the CHM, VCM, and the TM1 model give similar results at $\mu_B \lesssim 1.5$ GeV. All hadronic models predict the first order phase transition of the liquid–gas type at $\mu_B \simeq m_N$ which corresponds to baryon densities $\rho_B \lesssim \rho_0$. This is clear from Fig. 3 where pressure is shown at a finer scale. For example, in the case of the VCM the parts AB, BC, and AC of the pressure curve are unstable with respect to decomposition of matter into the dilute ($i = 1$) and dense ($i = 2$) phases. According to the Gibbs rules for coexisting phases

$$P^{(1)} = P^{(2)}\,, \tag{9}$$

$$\mu_B^{(1)} = \mu_B^{(2)}\,. \tag{10}$$

The phase transition points at $T = 0$ are given by intersection of different branches of pressure as a function of chemical potential[3]. For example, point A in Fig. 3 is the phase transition point in the case of the VCM.

According to Eq. (5), the density jump in the first order phase transition, $\rho_B^{(2)} - \rho_B^{(1)}$ is equal to the difference of slopes $dP/d\mu_B$ at $\mu_B \to \mu_c \pm 0$ where μ_c (the phase transition point) is the solution of Eq. (9). The equivalent criterion of the first order phase transition is the so–called "double tangent construction" for energy density as a function of baryon density. Indeed, by using thermodynamic identities (5)–(6) one can rewrite Eqs. (9)–(10) in the form

$$\frac{\epsilon^{(2)} - \epsilon^{(1)}}{\rho_B^{(2)} - \rho_B^{(1)}} = \frac{d\epsilon^{(1)}}{d\rho_B} = \frac{d\epsilon^{(2)}}{d\rho_B}\,. \tag{11}$$

Below the conditions (9)–(10) and (11) will be used for investigating the possibility and estimating parameters of the deconfinement transition by comparing pressures of hadronic ($i = 1$) and quark ($i = 2$) phases.

[3] When analyzing EOS in the $\mu_B - P$ plane one should bear in mind that lower branches of pressure correspond to metastable or unstable states.

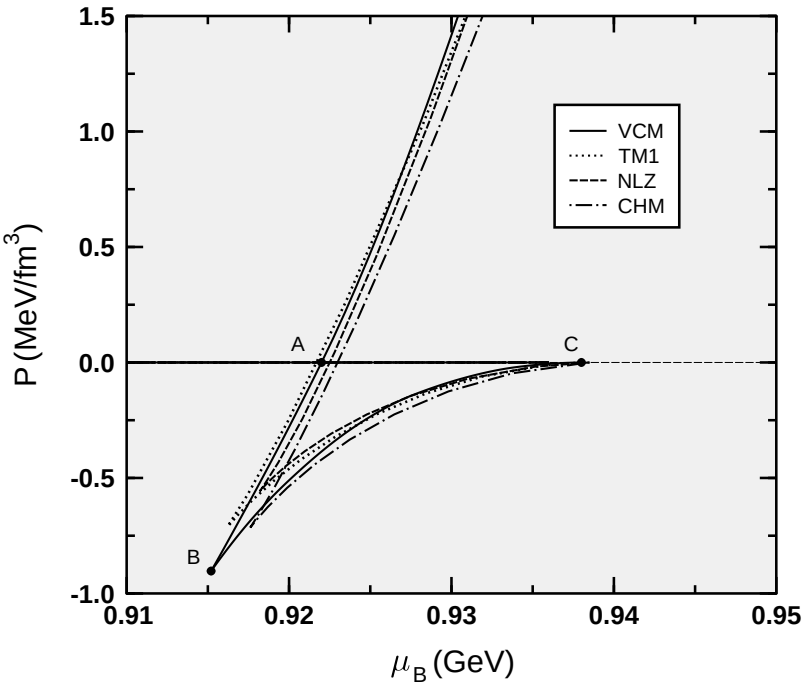

Figure 3: The same as in Fig. 2, but for small values of baryon chemical potential. Points A,B, and C show boundaries of metastable and unstable regions in the case of the VCM.

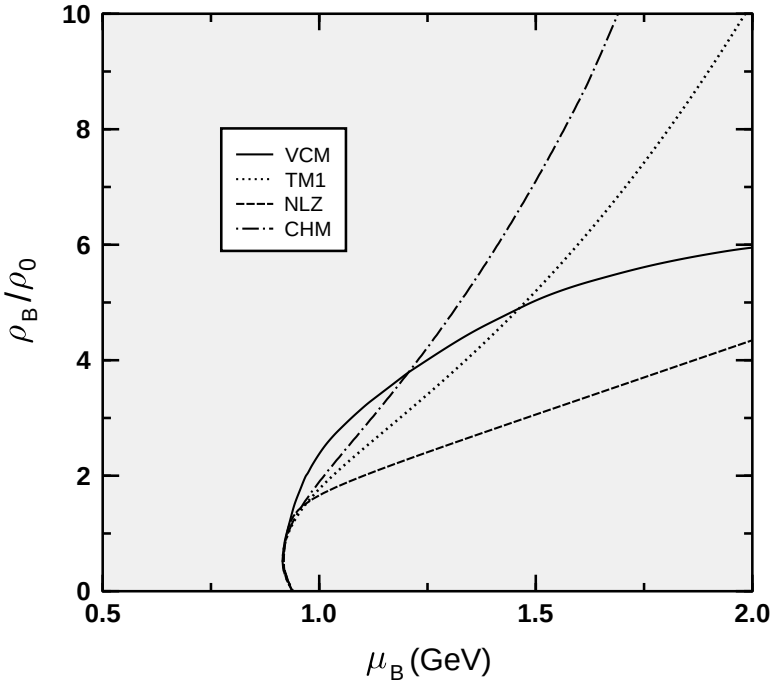

Figure 4: Baryon density of cold nuclear matter as function of chemical potential.

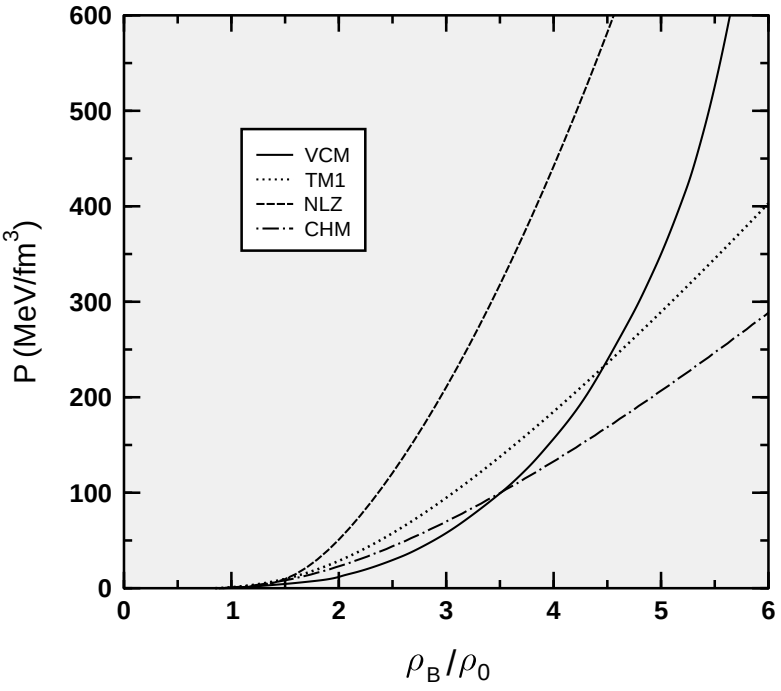

Figure 5: Pressure vs baryon density calculated within different hadronic models.

Four hadronic models considered in this paper predict essentially different behavior of the baryon density with raising μ_B. This is shown in Fig. 4. Again, one can see strong deviation of the NLZ results from the predictions of other hadronic models. Figure 5 shows pressure isotherms as functions of ρ_B. It is clearly seen that the NLZ model predicts the "hardest" EOS. Indeed, at intermediate densities $\rho_B \sim (1.5-4)\,\rho_0$ this model predicts the highest compressibility i.e. the largest derivative $dP/d\rho_B$. The NLZ model gives also the largest pressure at given ρ_B. On the other hand, the $P(\mu_B)$ curve predicted by this model is lower as compared to other models (see Fig. 2). Apparently, this difference is caused by the vector repulsion which is especially large in the NLZ model.

An important characteristic of nuclear matter is the in–medium nucleon mass m_N^*. Experiments on inelastic electron–nucleus scattering show that at $\rho_B \sim \rho_0$, this mass is lowered to about $0.7m_N$. By solving the gap equations (2), (7) one can calculate the ρ_B dependence of m_N^* within the CHM as well as in the TM1 and NLZ models. The results are shown in Fig. 6. All the models predict a rapid drop of m_N^* at $\rho_B \lesssim 2\rho_0$ and much slower decrease at higher densities. This behavior shows the tendency towards restoration of chiral symmetry at

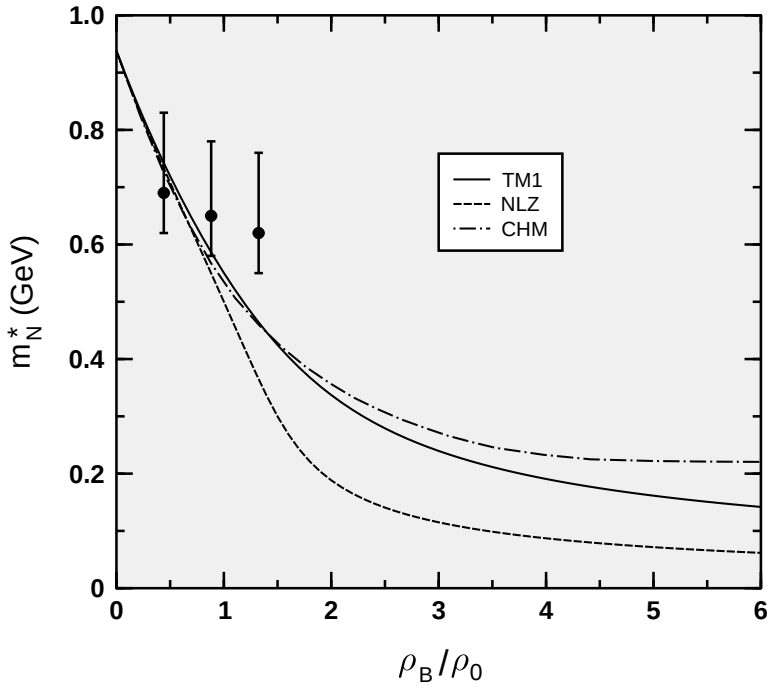

Figure 6: Nucleon effective mass as function of baryon density predicted by different hadronic models. The dots show estimates [15] obtained from the QCD sum rules.

high ρ_B .

Having in mind that predictions of the NLZ model at high densities strongly deviate from the results of other models, below we use only the CHM, VCM, and the TM1 model for the comparison with quark models.

3 Deconfined phase

3.1 The bag model

The simplest description of deconfined phase is given by the MIT bag model (BM). Within this model pressure of homogeneous nonstrange quark matter at zero temperature is expressed as

$$P = P_0(\mu) - B\,, \tag{12}$$

where $\mu = \mu_B/3$ is the chemical potential of light quarks, B is the bag constant and

$$P_0(\mu) = \frac{N_f \mu^4}{4\pi^2} \tag{13}$$

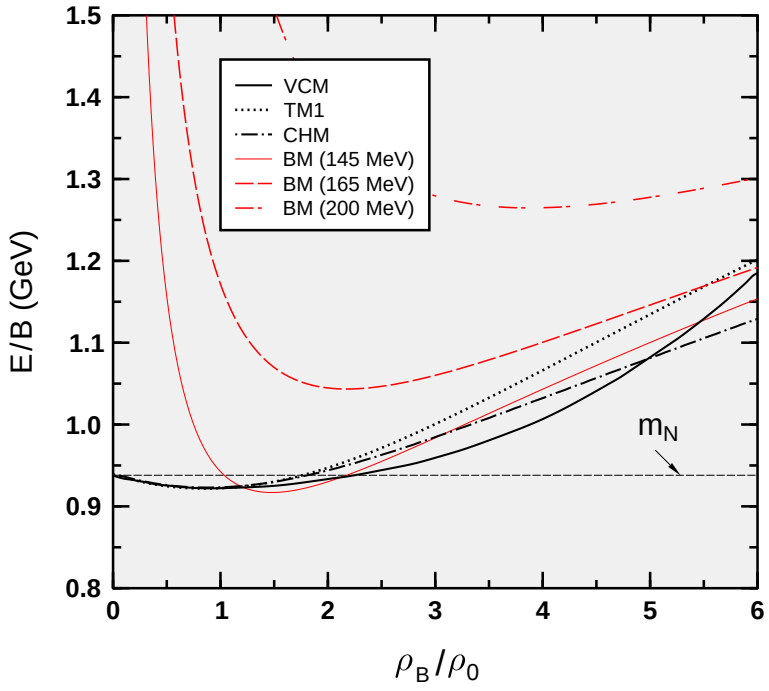

Figure 7: Comparison of energy per baryon of cold symmetric matter calculated within the MIT bag and different hadronic models. Values of $B^{1/4}$ in MeV are given in parentheses.

is pressure of ideal gas of massless quarks with N_f flavors. Below we assume that only light u, d quarks are present, i.e. $N_f = 2$. We consider the simplest version of the BM neglecting perturbative corrections due to the color–magnetic interaction. Thus, the only nonperturbative aspect of the model is associated with the bag constant B. The BM has been widely used for modelling a phase transition from the baryon–free hadron matter into the quark–gluon plasma at nonzero temperature. The critical temperature T_c for this transition is determined not only by the bag constant but also by the numbers of active degrees of freedom in respective phases. Reasonable values, $T_c \sim 160$ MeV, are obtained [16] with $B^{1/4} \sim 200$ MeV. The calculations below are made for $B^{1/4}$=145, 165 and 200 MeV.

In Figs. 7–9 we compare the EOS predicted by the hadronic models (VCM, CHM and TM1) and the BM for different values of B . Figure 7 shows energy per baryon as a function of baryon density. It is clear that small values of bag constant, $B^{1/4} \lesssim 150\,\mathrm{MeV}$, are unrealistic because in this case quark matter would be more stable at $\rho_B \sim \rho_0$ than cold nuclear matter. Due to this reason, below we consider only two values of bag constant corresponding to $B^{1/4} = 165$

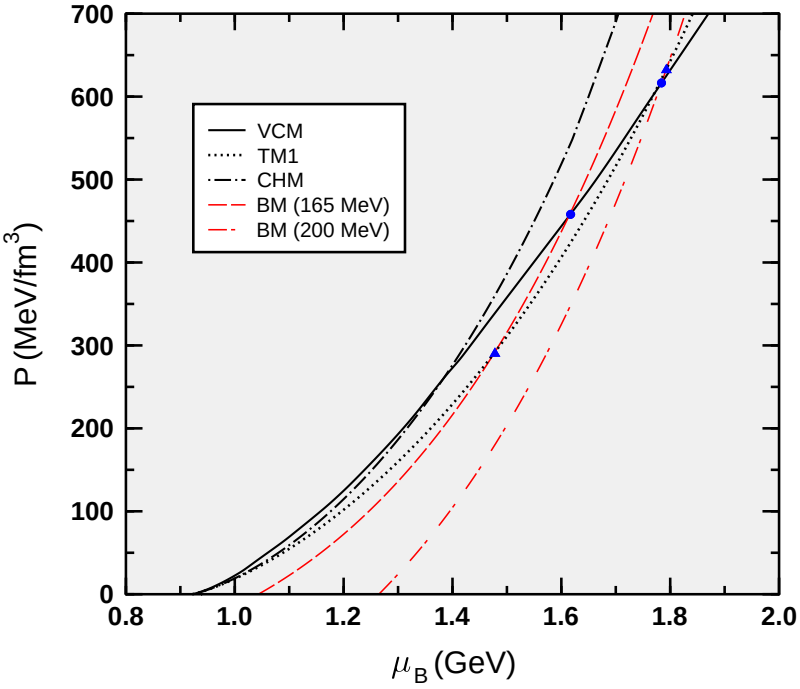

Figure 8: The same as in Fig. 7, but for pressure vs baryon chemical potential. Dots (triangles) mark the points of possible phase transitions from the VCM (TM1) hadronic phase to the BM quark phase with $B^{1/4} = 165$ and 200 MeV.

and 200 MeV.

Figure 8 shows pressure as a function of chemical potential calculated for the same models. From this figure one can see that at $B^{1/4} = 165$ and 200 MeV the transition from the hadronic to the quark phase is possible only for the VCM and the TM1 model. Filled symbols in Fig. 8 mark points of intersection between respective pressure curves. By using the Gibbs rules (9)–(10) it is possible to calculate parameters of the quark–hadron mixed phase predicted

Table 2: Parameters of hadron–quark phase transition predicted by matching the hadronic models and the BM with different bag constants B.

	$B^{1/4}$, MeV	μ_B, GeV	P, MeV/fm^3	$\rho_B^{(1)}/\rho_0$	$\rho_B^{(2)}/\rho_0$	$\epsilon^{(1)}$, GeV/fm^3	$\epsilon^{(2)}$, GeV/fm^3
TM1	165	1.478	292	5.02	6.19	0.97	1.20
TM1	200	1.793	634	7.86	11.04	1.76	2.73
VCM	165	1.617	458	5.35	8.10	1.01	1.77
VCM	200	1.783	615	5.66	10.84	1.10	2.67

by these models. The results of such calculation are summarized in Table 2. A more detailed

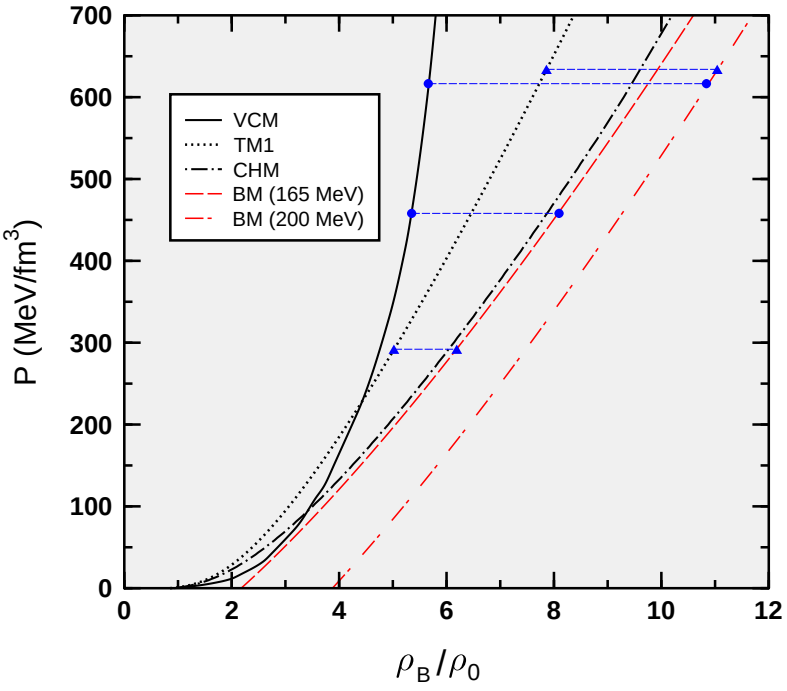

Figure 9: The same as in Fig. 7, but for pressure vs baryon density. Pairs of dots (triangles) connected by dashed lines show mixed hadron–quark states obtained by matching the EOS, predicted by the VCM (TM1 model) and the BM with $B^{1/4} = 165$ and 200 MeV.

information on the resulting EOS with the hadron–quark phase transition is given by Fig. 9. However, the calculations show that the phase transition occurs at rather large values of μ_B and ρ_B, in the region where applicability of hadronic models is questionable.

3.2 The massive quasiparticle model

A more realistic model of the quark phase, the MQM, has been proposed in Refs. [9, 10]. The case of hot baryon–free matter has been studied in Ref. [9]. In Ref. [10] a similar model was formulated to study the EOS of quark matter at $T = 0$, $\mu \neq 0$ [4]. Within the MQM it is assumed that cold quark matter may be regarded as an ideal gas of quarks with nonzero effective mass $m = m(\mu)$. Arguments in favor of this picture follow from calculations based on the hard thermal loop resummation technique developed in Refs. [17, 18, 19]. In the case of hot baryon–free matter it was possible to reproduce lattice results by using only leading order diagrams for quark and gluon self–energies. On the other hand, at small strong coupling

[4] It should be noted that the dependence of strong coupling constant on μ was disregarded in Ref. [10].

constant, $\alpha_s = g^2/4\pi$, one obtains results consistent with the perturbation theory up to the α_s^2 order. The case of cold quark matter has been recently studied [20] within the hard density loop resummation technique. It was shown that dependence of pressure on quark chemical potential can be well approximated by treating quarks as ideal gas of massive quasiparticles. However, the analytic formula $P = P_{\rm id}(m, \mu)$ suggested in Ref. [20] is thermodynamically inconsistent in the case when $m(\mu) \neq$ const (see below).

As shown in Refs. [21, 22, 23], at large enough 3–momenta the dispersion relation for quarks can be interpreted in terms of quasiparticles with nonzero effective mass m. In the leading order in α_s this mass can be expressed as [23]

$$m = \sqrt{\frac{2\alpha_s}{3\pi}}\,\mu\,. \tag{14}$$

One should have in mind that at small values of μ corresponding to $\alpha_s \gtrsim 1$ (see below) the applicability of Eq. (14) becomes questionable.

In our calculations we use the three–loop expression [24] for the strong coupling constant $\alpha_s = g^2/4\pi$ as function of the renormalization scale Q

$$\alpha_s(Q) = \frac{4\pi}{\beta_0 L}\left\{1 - \frac{2\beta_1}{\beta_0^2}\frac{\log L}{L} + \frac{4\beta_1^2}{\beta_0^4 L^2}\left[(L-1/2)^2 + \frac{\beta_0\beta_2}{8\beta_1^2} - \frac{5}{4}\right]\right\}. \tag{15}$$

Here $L = \log(Q^2/\Lambda^2)$ and

$$\beta_0 = 11 - 2\,N_f/3,\ \beta_1 = 51 - 19\,N_f/3,$$
$$\beta_2 = 2857 - 5033\,N_f/9 + 325\,N_f^2/27\,. \tag{16}$$

The cutoff momentum Λ is fixed by the condition $\alpha_s(2\,\mathrm{GeV}) = 0.3089$ [24], which gives $\Lambda \simeq 0.4178\,\mathrm{GeV}$ for $N_f = 2$. From dimensionality arguments it is clear that $Q \sim \mu$. As in Refs. [10, 20, 25], it is assumed that $Q = \gamma\mu$ where the coefficient γ is of the order of unity and does not depend on μ. At fixed γ physical values of μ correspond to $Q > \Lambda$.

Further it is postulated that the density of quark matter equals to the density of ideal gas of massive fermions

$$\rho = 3\rho_B = \rho_{\rm id}(\mu) \equiv \frac{N_f}{\pi^2}\left(\mu^2 - m^2\right)^{3/2}\Theta(\mu - m)\,, \tag{17}$$

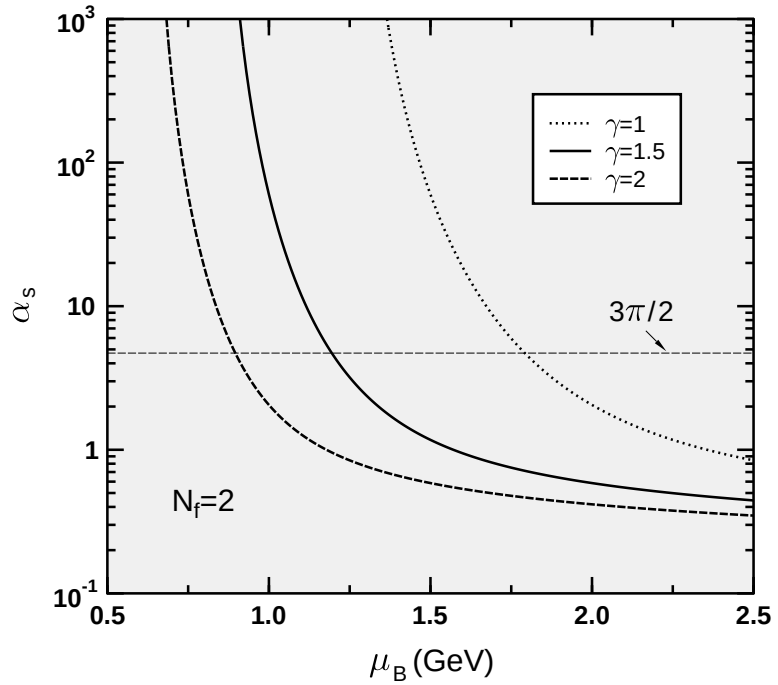

Figure 10: The QCD coupling constant as function of baryon chemical potential at $N_f = 2$ and different values of the parameter γ. Thin dashed line shows maximal possible value of α_s within the MQM.

where $\Theta(x) \equiv (1 + \mathrm{sgn}\, x)/2$. Thus, the quark density vanishes at $\mu \leq m$. This condition is satisfied at $\mu \leq \mu_c$ where μ_c is the critical chemical potential determined from Eq. (14) with $m = \mu$. The latter condition is equivalent to $\alpha_s = 3\pi/2$. The calculation shows that $\mu_c \simeq 0.5974/\gamma$ GeV for $N_f = 2$.

Figs. 10–11 show α_s and m as functions of baryon chemical potential $\mu_B = 3\mu$ for several values of the parameter γ. The shaded region in Fig. 11 corresponds to the domain where $m > \mu$. It is seen that quark masses are very sensitive to the choice of γ. At large μ_B quark masses increase, although slower than μ_B. As discussed in Ref. [26], the existence of nonzero quark mass does not contradict to the restoration of chiral symmetry at large μ_B.

Using Eq. (17) and thermodynamic identity (5) one can calculate pressure as a function of μ:

$$P = \int\limits_{\mu_c}^{\mu} \mathrm{d}\mu_1 \rho_{\mathrm{id}}(\mu_1)\,. \tag{18}$$

Here we assume that $P(\mu_c) = 0$, i.e. pressure is zero at vanishing quark density. If one

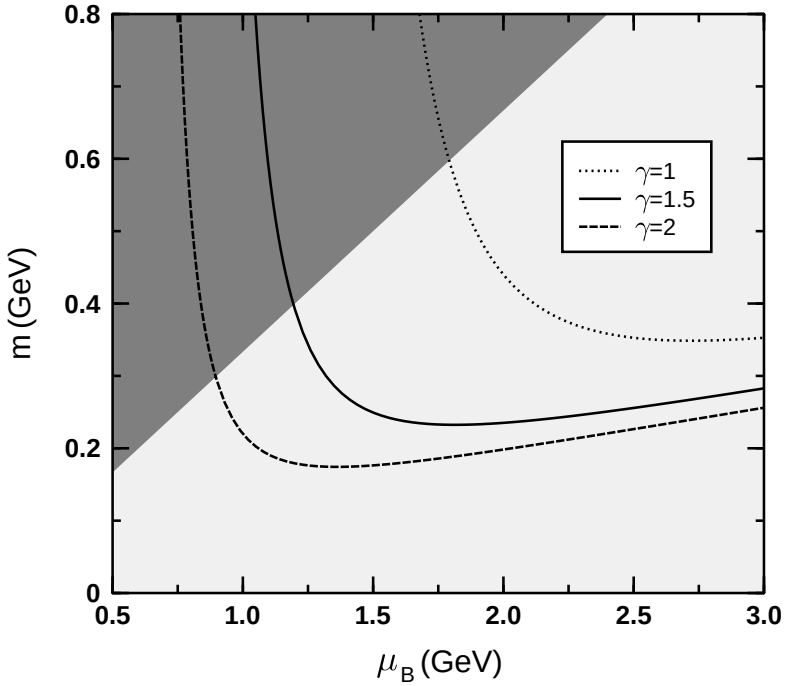

Figure 11: Effective mass of u, d quarks m within the MQM vs baryon potential of quark matter μ_B. Unphysical region is shown by shading.

would replace $m(\mu_1)$ in the integrand $\rho_{\rm id}$ by the "constant" mass $m(\mu)$, one would obtain the well–known expression [20] for pressure of ideal gas $P_{\rm id}$. However, as shown in Ref. [27], the approximation $P = P_{\rm id}$ is thermodynamically inconsistent when masses depend on T or μ_B. In particular, Eq. (5) does not hold in this case. The thermodynamic consistency can be recovered by introducing the effective bag constant $B(\mu) = P_{\rm id} - P$.

Figure 12 shows thermodynamic quantities calculated within the MQM by using Eqs. (17)–(18), (6). Density, pressure and energy density are shown as functions of the dimensionless variable μ/μ_c. All quantities are given as ratios to their respective limits for massless quarks ($P_{SB} = \epsilon_{SB}/3 = P_0(\mu)$). In this representation the results do not depend on γ. In Fig. 12 we also demonstrate inaccuracy of the approximation $P = P_{\rm id}$ used in Ref. [20]. It is seen that $B(\mu)$ is typically of order $0.1P_{\rm id}$ and changes sign at $\mu \sim 2\mu_c$.

Energy per baryon and pressure calculated within the MQM are compared with predictions of hadronic models in Figs. 13–14. Unlike the BM, in this model the energy per baryon increases

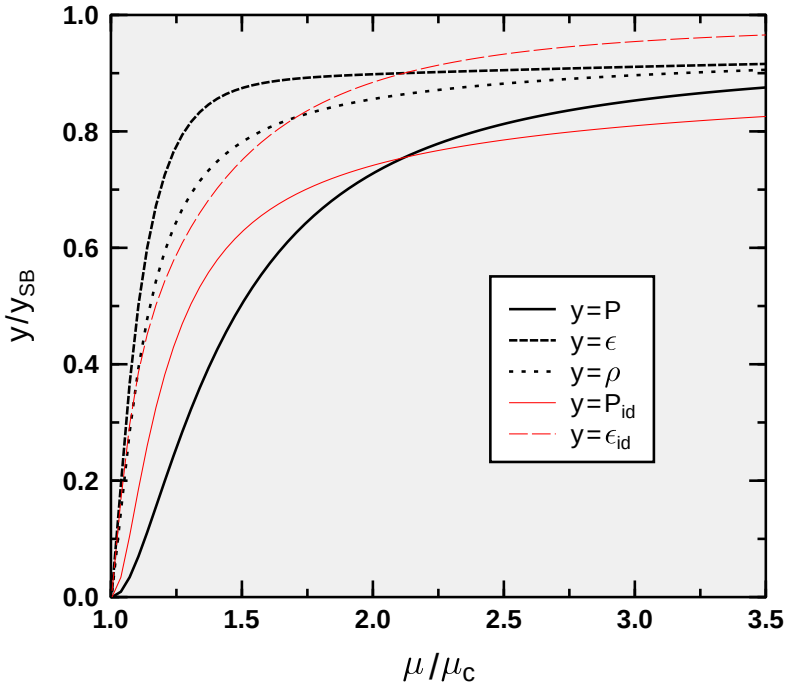

Figure 12: Pressure P, energy density ϵ and number density ρ of quarks within the MQM (normalized to their Stephan–Boltzmann limits, $m \to 0$) as functions of quark chemical potential μ in units of its critical value μ_c. Thin solid and dashed lines show pressure and energy density calculated by using the ideal gas approximation $B(\mu) = 0$.

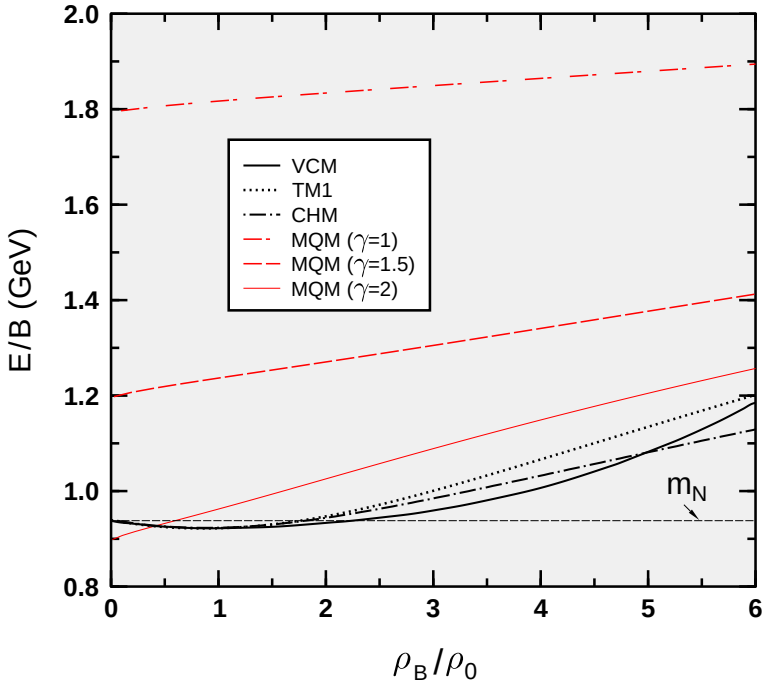

Figure 13: Comparison of energy per baryon of cold symmetric matter calculated within the MQM and different hadronic models.

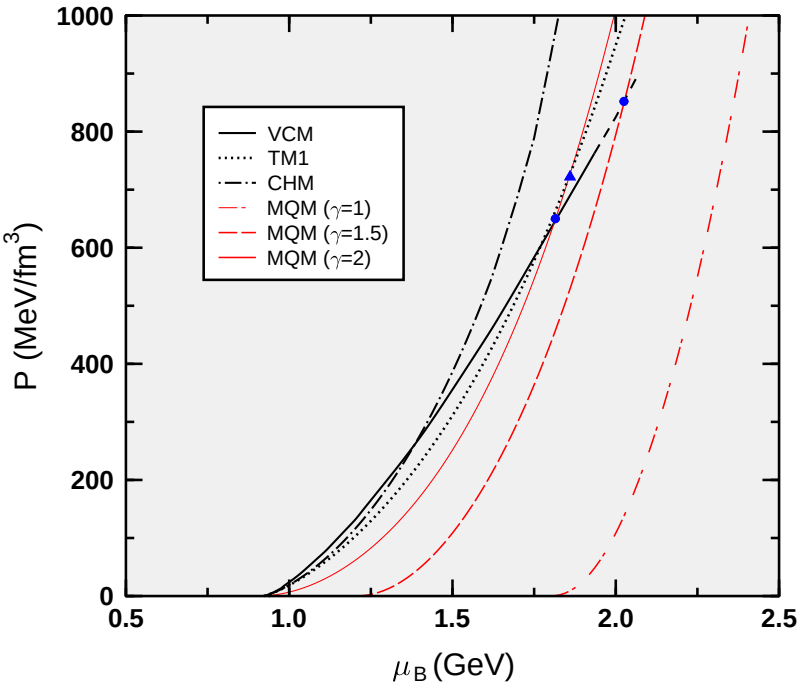

Figure 14: The same as in Fig. 13, but for pressure vs baryon chemical potential. Filled symbols show points of possible phase transitions.

monotonically with ρ_B, even at low densities. According to Fig. 13, the MQM with $\gamma > 2$ is unrealistic since in this case the quark matter would be energetically more favorable at $\rho_B \lesssim \rho_0$ than normal nuclear matter.

According to Fig. 14 at $1.5 \leq \gamma \leq 2$ the MQM pressure curve intersects only with curves predicted by the VCM and the TM1 model. Parameters of possible phase transitions are given in Table 3. One can see that quark phase appears only at rather high baryonic densities, namely, at $\rho_B > \rho_B^{(1)} \gtrsim 6\rho_0$. At $\gamma \lesssim 1$ there are no intersections of hadronic and quark branches, at least at not too large μ_B.

Table 3: Parameters of quark–hadron phase transition predicted by matching the VCM, TM1 model, and MQM at different γ.

γ	μ_B, GeV	P, MeV/fm^3	$\rho_B^{(1)}/\rho_0$	$\rho_B^{(2)}/\rho_0$	$\epsilon^{(1)}$, GeV/fm^3	$\epsilon^{(2)}$, GeV/fm^3
1.5 (VCM)	2.025	852	6.0	13.2	1.21	3.71
2.0 (VCM)	1.815	650	5.7	9.1	1.11	2.17
2.0 (TM1)	1.860	725	8.6	10.6	1.95	2.67

We have also checked sensitivity of the results to the choice of N_f in the QCD coupling constant. The calculation has been made using $N_f = 3$ in Eqs. (15)–(16), but retaining $N_f = 2$ (only u and d quarks) in thermodynamic quantities. This leads to a slight increase of $P(\mu_B)$ that lowers the phase transition density by not more than 10%.

3.3 The Nambu–Jona-Lasinio model

The NJL model [11, 12] is one of the most popular models dealing with constituent quarks. There are several advantages of the NJL model compared to other models considered above. First, it respects chiral symmetry of strong interactions, second, it explicitly takes into account negative energy (Dirac sea) states, and third, it describes well meson phenomenology. Different versions of this model have been extensively used to describe the EOS of equilibrium and nonequilibrium quark matter at finite T and μ_B .

Here we use results of our calculations [28, 29, 30] within the SU(3)–flavor version of the model suggested in Ref. [31], but with an additional term due to vector–axial-vector interaction. The color-singlet part of the Lagrangian in the mean field approximation can be written as

$$\begin{aligned} \mathcal{L} &= \sum_f \overline{\psi}_f \left(i\partial\!\!\!/ - m_f - \gamma_0 G_V \rho_{Vf} \right) \psi_f - \frac{G_S}{2} \sum_f \rho_{Sf}^2 \\ &+ \frac{G_V}{2} \sum_f \rho_{Vf}^2 + 4K \prod_f \rho_{Sf} \, . \end{aligned} \tag{19}$$

Here ψ_f is the field operator of quarks with flavor $f = u, d, s$ and

$$\rho_{Sf} = < \overline{\psi}_f \psi_f > , \tag{20}$$

$$\rho_{Vf} = < \overline{\psi}_f \gamma_0 \psi_f > \tag{21}$$

are their scalar and vector densities. Angular brackets in Eqs. (20)–(21) denote quantum–statistical averaging. G_S, G_V and K in Eq. (19) are, respectively, the coupling constants of scalar, vector and flavor–mixing interactions.

The constituent quark masses, m_f, are determined from the coupled set of gap equations

$$m_f = m_{0f} - G_S \, \rho_{Sf} + 2K \prod_{f' \neq f} \rho_{Sf'} \, , \tag{22}$$

where m_{0f} is the bare (current) mass of quarks with flavor f.

The NJL model is an effective, non–renormalizable model. To regularize the divergent contribution of negative energy states of the Dirac sea, one must introduce an ultraviolet cut–off. Below the 3–momentum cut–off $\Theta(\Lambda - p)$ is used in divergent integrals. The model parameters m_{0f}, G_S, K, Λ can be fixed by reproducing the observed masses of π, K, and η' mesons as well as the pion decay constant. As shown in Ref. [31], a reasonable fit is achieved with the following input parameters:

$$m_{0u} = m_{0d} = 5.5 \text{ MeV}, \quad m_{0s} = 140.7 \text{ MeV}, \tag{23}$$

$$G_S = 20.23 \text{ GeV}^{-2}, \qquad \Lambda = 0.6023 \text{ GeV}, \qquad K = 155.9 \text{ GeV}^{-5}. \tag{24}$$

In principle, the vector coupling constant may be extracted by fitting the nucleon axial charge or masses of vector mesons. It was shown [32] that the ratio $\xi = G_V/G_S$ should be of the order of unity. However, as discussed in Ref. [33], the accuracy of such fitting procedure is rather low. Due to uncertainty in the parameter G_V, below we present results for various values of ξ from the interval $0 \le \xi \le 1$.

Let us consider cold isospin–symmetric nonstrange matter with baryon density ρ_B. In this case $\rho_{Vs} = 0, \rho_{Vu} = \rho_{Vd} = 3\rho_B/2$. The energy density ϵ can be calculated directly from the Lagrangian (19) with the result [29]

$$\epsilon = \sum_f \left[\epsilon_{Kf} + \frac{G_S}{2}\rho_{Sf}^2 + \frac{G_V}{2}\rho_{Vf}^2 \right] - 4K \prod_f \rho_{Sf} + \epsilon_0 \,. \tag{25}$$

Here ϵ_{Kf} is the kinetic term which includes also "active" negative energy states with momenta $p < \Lambda$:

$$\epsilon_{Kf} = \frac{3}{\pi^2} \int_\Lambda^{p_{Ff}} \mathrm{d}p \, p^2 \sqrt{m_f^2 + p^2} \,, \tag{26}$$

where $p_{Ff} = (\pi^2 \rho_{Vf}/3)^{1/3}$ is the f–quark Fermi–momentum. Scalar densities can be calculated by using the relation

$$\rho_{Sf} = \left(\frac{\partial \epsilon_{Kf}}{\partial m_f} \right)_{p_{Ff}} . \tag{27}$$

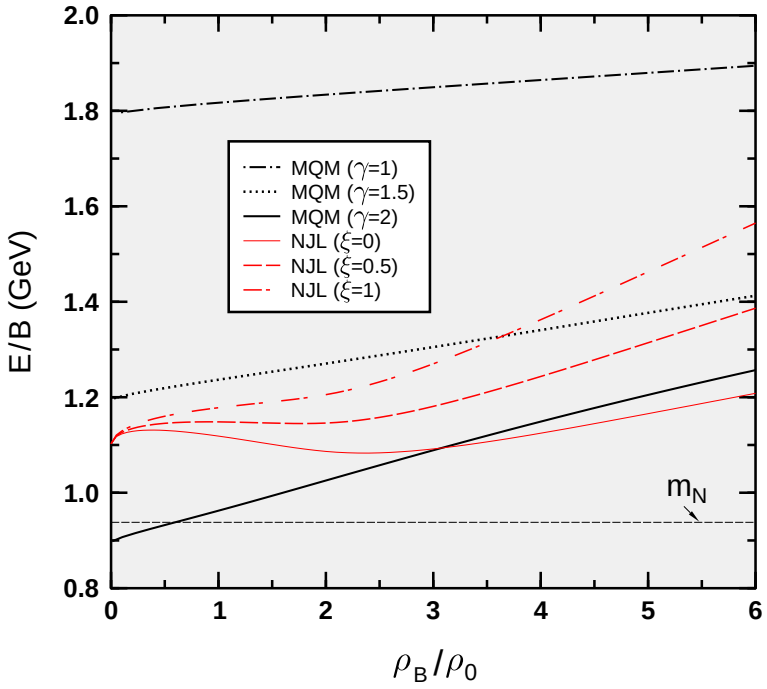

Figure 15: Comparison of energy per baryon of cold symmetric matter calculated within the MQM and NJL model.

The constant ϵ_0 in the l.h.s. of Eq. (25) is introduced in order to set the energy density of the physical vacuum equal to zero. This constant can be calculated by solving the gap equations (22) for the vacuum case, $\rho_B = 0$. Finally, pressure can be found by using thermodynamic identities $\mu_B = d\epsilon/d\rho_B$ and $P = \mu_B\rho_B - \epsilon$.

The results of calculations are shown in Figs. 15–18 for three values (0, 0.5, 1.0) of the parameter ξ. Figs. 15–16 show the comparison of the MQM and NJL model. It is seen that the discrepancy between their results is especially large in the case $\gamma = 1$. Unlike the MQM, the NJL model predicts metastable states of quark matter corresponding to local minima in E/B as function of ρ_B. However, such states exist only at $\xi \lesssim 0.1$ [5].

In Figs. 17–18 we compare EOS predicted by the NJL and hadronic models. As seen in Fig. 18 the hadron–quark phase transition may take place only at small ξ which, most likely, are not realistic. For larger ξ the repulsive vector interaction makes the NJL phase too stiff to cross any of the hadronic curves. The phase transition parameters for $\xi = 0$ are given in Table 4.

[5] As shown in Refs. [29, 30], they appear in strange matter even at larger ξ.

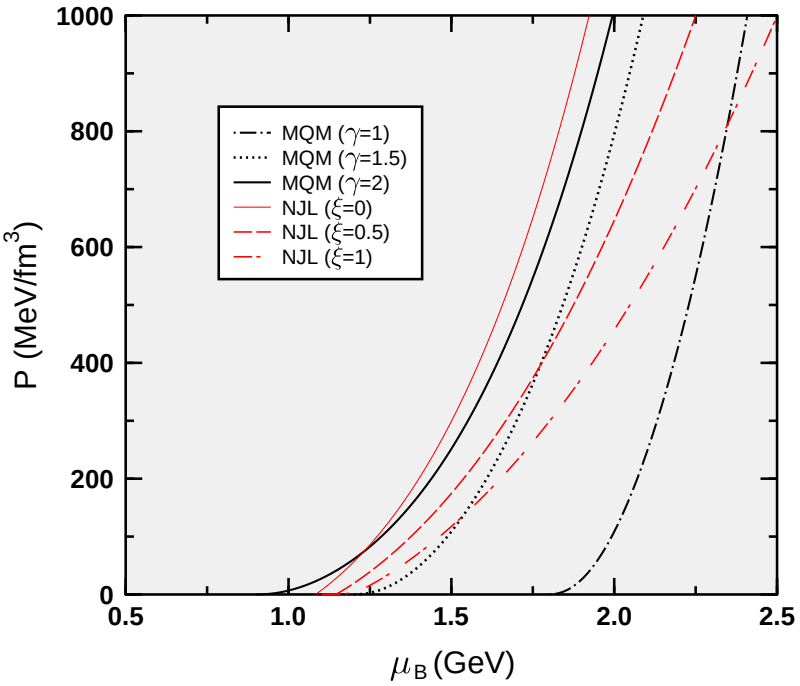

Figure 16: The same as in Fig. 15, but for pressure vs baryon chemical potential.

Again the transition to quark matter is possible only from the TM1 and VCM hadronic phases and predicted critical densities are above $5\rho_0$.

At $\xi < 0.71$ the pressure isotherms calculated within the NJL model contain unstable parts in the region $\mu_B \simeq 1 - 1.2$ GeV [29]. This means that this model itself predicts the first-order chiral phase transition in the quark matter. However, corresponding parts of pressure isotherms lie below the hadronic curves. Therefore, such a phase transition is not observable due to the hadronization of quark phase. This situation is quite general: many phase transitions found within different quark models are predicted in regions of the $\mu_B - P$ plane where quark phase is unstable with respect to hadronization.

Table 4: Parameters of hadron–quark phase transition matching the VCM and TM1 model with the NJL model ($\xi = 0$).

	μ_B, GeV	P, MeV/fm^3	$\rho_B^{(1)}/\rho_0$	$\rho_B^{(2)}/\rho_0$	$\epsilon^{(1)}$, GeV/fm^3	$\epsilon^{(2)}$, GeV/fm^3
TM1–NJL	1.555	363	5.6	7.2	1.18	1.54
VCM–NJL	1.646	487	5.4	8.5	1.02	1.89

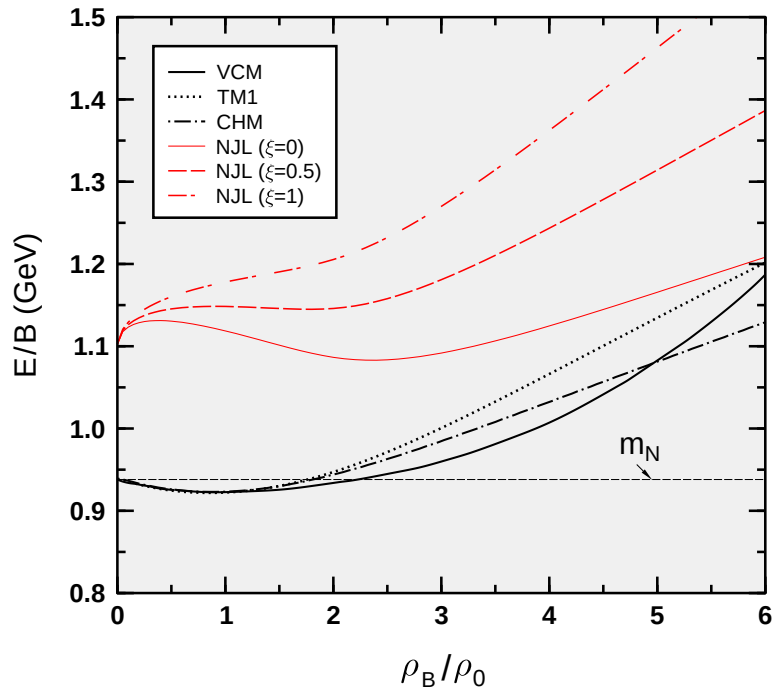

Figure 17: Comparison of energy per baryon of cold symmetric matter calculated within the NJL model and different hadronic models.

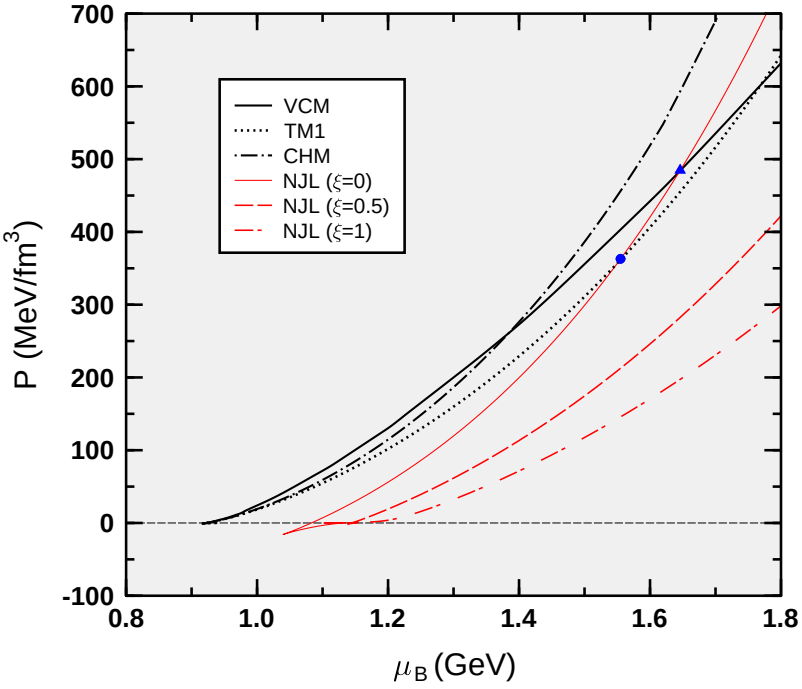

Figure 18: The same as in Fig. 17, but for pressure vs baryon chemical potential. Filled symbols show points of possible phase transitions.

4 Conclusions and outlook

Our goal in this paper was to find possible phase transition between hadronic and quark phases of strongly interacting matter at high baryon density. For each of the phases we have selected several models which are widely discussed in the literature. Namely, we have considered the CHM, VCM, and RFM models for the hadronic phase, and the BM, MQM, and NJL model for the quark phase. When necessary, we have varied model parameters in reasonable limits to determine possible range of uncertainty. For each model we have calculated main thermodynamic quantities, in particular, pressure as a function of baryon chemical potential, $P(\mu_B)$. Possibility of a deconfinement phase transition is signalled by an intersection of $P(\mu_B)$ curves corresponding to the hadronic and quark phases.

A pairwise comparison of different hadronic and quark models has shown that such an intersection is not at all a general feature but rather an exception. For instance, the CHM, which is probably the most advanced hadronic model at present, does not predict a phase transition with any of quark models. Also, no phase transition is predicted when most realistic parameters are used in quark models ($B^{1/4} \simeq 200$ MeV in the BM, $\gamma \simeq 1$ in the MQM, or $\xi \gtrsim 0.5$ in the NJL model). Even in the cases when a phase transition is possible, e.g. between the TM1 model and the BM, or between the VCM and BM, characteristics of mixed phase are very sensitive to model parameters. Moreover, this phase transition is predicted at such a high density, above $5\rho_0$ where predictions of hadronic models are very unreliable. The situation with quark models is even worse. First, it is unclear at all how far down in density one can use these models. Second, the predictions of various quark models differ significantly in the region of moderately high baryon densities of interest here. Of course, due to the asymptotic freedom of QCD the quark phase must approach asymptotically the ideal gas limit. However, it is unclear at present when such asymptotic behavior sets in.

In this paper we have considered only isospin–symmetric matter, but we think that similar conclusions can be made also for β–equilibrium neutron star matter. For example, the comparison of EOS predicted by the CHM and NJL model (for details see Ref. [33]) does not show

any phase transition between hadronic and quark phases.

As has been demonstrated in this paper, some phase transitions found in the QCD motivated models, e.g. the chiral transition within the NJL model, occupy regions of the $\mu_B - P$ plane where quark phases are unstable with respect to hadronization. We expect that similar situation takes place also for color-superconducting phases of quark matter [34, 35], although this question deserves a special study.

We should conclude that after more than 30 years of model building in both the hadronic and quark sectors the situation regarding a hadron–quark phase transition and EOS at high baryon densities remains rather uncertain. We believe that progress in this field can be achieved by developing new class of models where both the hadronic and quark degrees of freedom are treated within a unified theoretical framework. Attempts to construct such a model were made in Refs. [36, 37]. Such unified approach should include constraints from nuclear physics (existence of the nuclear bound state) and QCD (chiral symmetry, asymptotic freedom). It is quite possible that the transition from hadronic to quark degrees of freedom will be continuous [29], like ionization in atomic systems [38]. Indications of such behavior are found in recent lattice calculations [39]. All this means that the problem of hadron–quark transition at high baryon densities remains a challenge for theorists.

Acknowledgments

The authors thank P.J. Ellis and D.H. Rischke for fruitful discussions. I.N.M. and L.M.S. acknowledge financial support from DAAD and GSI, Germany. This work has been partially supported by the RFBR Grant No. 00–15–96590.

References

[1] B.D. Serot and J.D. Walecka, Adv. Nucl. Phys. **16**, 1 (1985).

[2] B.D. Serot and J.D. Walecka, Int. J. Mod. Phys. **E6**, 515 (1997).

[3] M. Rufa et al., Phys. Rev. C **38**, 390 (1989).

[4] Y. Sugahara and H. Toki, Nucl. Phys. **A579**, 557 (1994).

[5] P. Papazoglou, S. Schramm, J. Schaffner–Bielich, H. Stöcker, and W. Greiner, Phys. Rev. C **57**, 2576 (1998).

[6] P. Papazoglou, D. Zschiesche, S. Schramm, J. Schaffner–Bielich, H. Stöcker, and W. Greiner, Phys. Rev. C **59**, 411 (1999).

[7] A. Akmal, V.R. Pandharipande, and D.G. Ravenhall, Phys. Rev. C **58**, 1804 (1998).

[8] A. Chodos, R.L. Jaffe, K. Johnson, C.B. Thorn, and V.F. Weisskopf, Phys.Rev. D **9**, 3471 (1974).

[9] A. Peshier, B. Kämpfer, O.P. Pavlenko, and G. Soff, Phys. Rev. D **54**, 2399 (1996).

[10] K. Schertler, C. Greiner, and M.H. Thoma, Nucl. Phys. A **A616**, 659 (1997).

[11] Y. Nambu and G. Jona–Lasinio, Phys. Rev. **122**, 345 (1961); **124**, 246 (1961).

[12] V.G. Vaks and A.I. Larkin, Sov. J. JETP **13**, 192 (1961).

[13] E.K. Heide, S. Rudaz, and P.J. Ellis, Nucl. Phys. **A571**,713 (1994).

[14] I.N. Mishustin, J.P. Bondorf, and M. Rho, Nucl. Phys. **A555**, 213 (1993).

[15] R.J. Furnstahl, X. Jin, and D.B. Leinweber, Phys. Lett. B **387**, 253 (1996).

[16] I.J. Kapusta, *Finite–temperature field theory*, Cambridge Press, NY, 1984.

[17] F. Karsh, A. Patcós, and P. Petreczky, Phys. Lett. B **401**, 69 (1997).

[18] J.-P. Blaizot, E. Iancu, and A. Rebhan, Phys. Lett. B **470**, 181 (1999);
Phys. Rev. D **63**, 065003 (2001).

[19] J.O. Andersen, E. Braaten, and M. Strickland, Phys. Rev. Lett. **83**, 2139 (1999).

[20] R. Baier and K. Redlich Phys. Rev. Lett. **84**, 2100 (2000).

[21] V.V. Klimov, Sov. J. JETP **55**, 199 (1982).

[22] H.A. Weldon, Phys. Rev. D **26**, 1394 (1982).

[23] K. Kajantie and P.V. Ruuskanen, Phys. Lett. B **121**, 352 (1983).

[24] D.E. Groom et al., Eur. Phys. J. **C15**, 1 (2000).

[25] E.S. Fraga, R.D. Pisarski, and J. Schaffner–Bielich, Phys. Rev. D **63**, 121702 (2001).

[26] H.A. Weldon, Phys. Rev. D **26**, 2789 (1982).

[27] M.I. Gorenstein and S.N. Yang, Phys. Rev. D **52**, 5206 (1995).

[28] I.N. Mishustin, L.M. Satarov, H. Stöcker, and W. Greiner, Phys. Rev. C **59**, 3343 (1999).

[29] I.N. Mishustin, L.M. Satarov, H. Stöcker, and W. Greiner, Phys. Rev. C **62**, 034901 (2000).

[30] I.N. Mishustin, L.M. Satarov, H. Stöcker, and W. Greiner, Phys. Atom. Nucl. **64**, 802 (2001).

[31] P. Rehberg, S.P. Klevansky, and J. Hüfner, Phys. Rev. C **53**, 410 (1996).

[32] S. Klimt, M. Lutz, and W. Weise, Phys. Lett. **B249**, 386 (1990).

[33] M. Hanauske, L.M. Satarov, I.N. Mishustin, H. Stöcker, and W. Greiner, Phys. Rev. D **64**, 043005 (2001).

[34] M. Alford, K. Rajagopal, and F. Wilczek, Phys. Lett. B **422**, 247 (1998).

[35] T.M. Schwarz, S.P. Klevansky, and G. Papp, Phys. Rev. C **60**, 055205 (1999).

[36] E.G. Nikonov, V.D. Toneev, and A.A. Shanenko, Phys. Atom. Nucl. **62**, 1226 (1999).

[37] K. Schwenzer, J. Meyer, and H.J. Pirner, Phys. Lett. B **473**, 25 (2000).

[38] L.D. Landau and E.M. Lifshitz, *Statistical physics*, Pergamon Press, 1980.

[39] J. Engels, O. Kaczmarek, F. Karsch, and E. Laermann, Nucl. Phys. B **558**, 307 (1999).